Electronic supplementary information

S1 Determining the friction correction γ_s
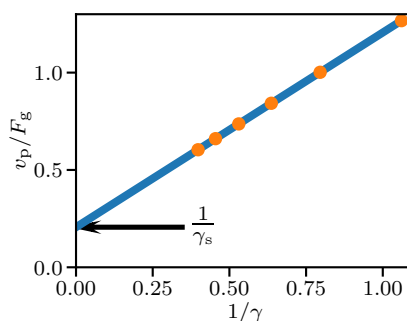

Figure S1: Single-particle velocity v_p under constant force F_g as a function of the uncorrected friction coefficient $\gamma = 6\pi\mu R$ used to obtain γ_s for the Peskin stencil. Circles mark simulation data and the blue line is a linear fit.

Using γ_s instead of γ to calculate the friction force acting on a particle in the fluid flow effectively substracts the Stokeslet contribution of the particle from the actual local fluid velocity. γ_s is equal to the y-intercept at $1/\gamma \to 0$ in Fig. S1.[1] There are no data points at small values of $1/\gamma$ because the particle-fluid coupling is numerically unstable for particle radii approaching or exceeding the size of the stencil.

---

[1] S. Ollila, C. Smith, T. Ala-Nissila and C. Denniston, *Multiscale Model. Simul.*, 2013, **11**, 213–243.

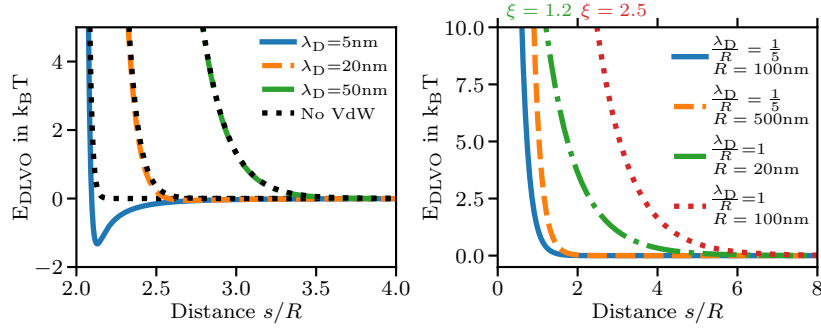## S2 DLVO potential and repulsive range χ

Figure S2: Left: Total DLVO potential compared to only the repulsive part in water for different Debye lengths with $R = 300\,\text{nm}$ and $\zeta = 50\,\text{mV}$. Right: Radius dependence of the repulsive DLVO potential at fixed distance s/R and Debye length λ_D/R in units of the radius. Significantly different values of ξ (distance, where the repulsive potential exceeds $10\,\text{k}_\text{B}\text{T}$) are needed to approximate the system using Eq. (21) depending on R, particularly when $\lambda_\text{D} \gtrsim R$.

S3 Radius dependence of repulsive potential

Let $R' = aR$, with $a > 1$, $\hat{\lambda}_\text{D} = \lambda_\text{D}/R$ and $\hat{s} = \hat{\lambda}_\text{D} + \epsilon$ with $\epsilon > 0$. Then, according to Eq. (15), $E'_\text{coul}(\hat{s} = s'/R')$ for a particle of radius R' is smaller as compared to $E_\text{coul}(\hat{s} = s/R)$ for a particle of smaller radius R, all other variables being equal, if

$$\frac{E'_\text{coul}}{E_\text{coul}} = \frac{R'}{R}\text{e}^{-\frac{\hat{\lambda}_\text{D}+\epsilon}{\lambda_\text{D}}(R'-R)} = a\text{e}^{-\frac{\hat{\lambda}_\text{D}+\epsilon}{\hat{\lambda}_\text{D}}(a-1)} < 1. \tag{S1}$$

We can use the fact that all terms in the Taylor series of an exponential function with positive argument are also positive to rewrite the inequality in Eq. (S1) as

$$(a-1) < \frac{\hat{\lambda}_\text{D}+\epsilon}{\hat{\lambda}_\text{D}}(a-1), \tag{S2}$$

which is always true under the above-mentioned conditions.

S4 Velocity and linear fit errors

We repeated simulations with different random initial particle placements at a range of values of χ and calculated the errors $\Delta v/v_0$ in average sedimentation velocity and ΔK in slope as the standard deviations of the results of these runs.
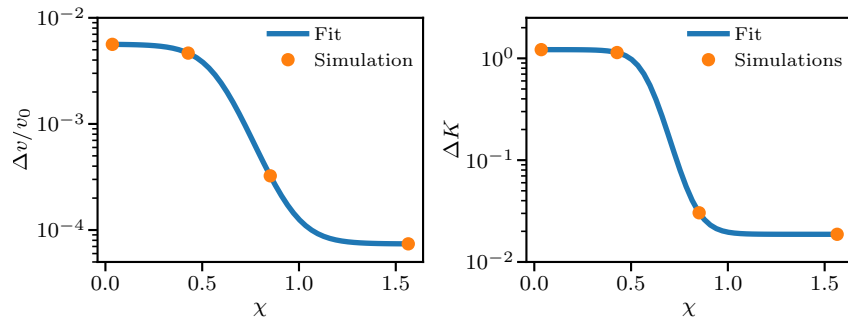
Figure S3: Change of error in measured velocities (left) and the derived slope K (right) as a function of χ. Each data point represents an averaged value obtained over four concentrations from 0.2-0.8% with 4-6 repetitions of each simulation. The first data point at $\chi \approx 0$ results from averaging over a total of seven such sets of simulations at similar values of χ but different parameters. Like the error itself, the uncertainty in the error is also higher for lower χ.

For simulation parameters at which we performed no averaging, we instead estimated the errors from fits of $\Delta v/v_0$ and ΔK as functions of χ. The fits, shown in Fig. S3, follow a logistic curve with a drastic decrease by about two orders of magnitude in the errors in the region of $\chi = 0.5-1$, where the particles transition into an ordered state.

We also measured the single particle velocity v_0 in sedimentation direction under random particle placement in each simulation setup used for our sedimentation simulations and averaged these measurements. Since we simulated approximately the same number of particles in each simulation, the system size has to vary with concentration. This in turn leads to a changing degree of influence of the periodic boundaries on the single particle. Also its position with respect to the lattice can have a small ($< 1\%$) influence on the obtained steady-state velocity.[2] We observed a standard deviation among these measurements of $\sqrt{\langle v_0^2 \rangle - \langle v_0 \rangle^2}/\langle v_0 \rangle = 0.24\%$. The averaged v_0 deviates from the theoretical Stokes velocity by about 1% due to the above reasons and presumably due to small inaccuracies in the calibration of γ_s. Most of the uncertainty in our results seems to stem from the finite sample size of 10 000 particles and the randomness involved in their initial placement and subsequent evolution under Langevin dynamics.

S5   Reconstructing the hindrance function

The hindrance function $v(\phi)/v_0$ can be reconstructed from the fitted slope $K(\chi)$ (Eq. (27)) by numerical integration. For this purpose we interpret K as the slope

[2]S. Ollila, C. Smith, T. Ala-Nissila and C. Denniston, *Multiscale Model. Simul.*, 2013, **11**, 213–243.
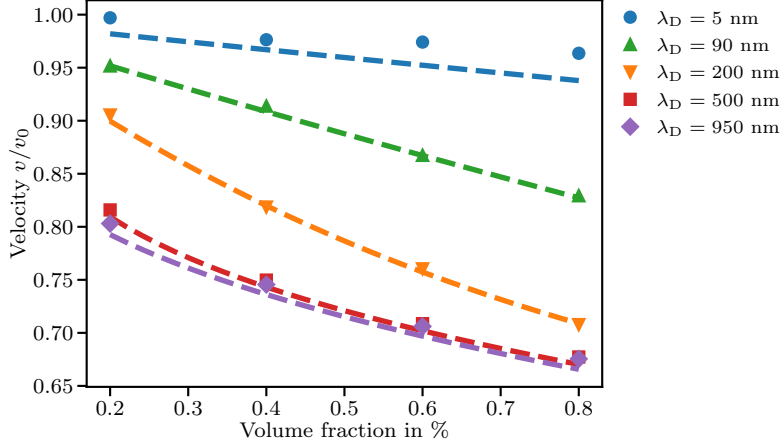
Figure S4: Sedimentation velocity of DLVO-interacting particles with radius $R = 200\,\text{nm}$ at various Debye lengths compared to predictions from Eq. (S4).

of $-v(\phi)/v_0$ at a discrete value of ϕ, rather than as the result of linear fitting over a range of ϕ. Hence we substitute K_ω in Eq. (27) by the derivative K_∂ of $-v(\phi)/v_0$ with respect to ϕ, with $v(\phi)$ described by the power law form valid for ordered suspensions (Eq. (18)), so that

$$K_\partial = -\frac{\partial}{\partial \phi}\frac{v(\phi)}{v_0} = \frac{\varsigma}{\omega}\phi^{\frac{1}{\omega}-1}. \tag{S3}$$

Inserting the modified Eq. (27) for K, the hindrance function can be calculated as

$$\frac{v(\varphi)}{v_0} = 1 - \int_0^\varphi K(\xi,\phi)\,\mathrm{d}\phi = 1 - \int_0^\varphi (K_\Phi(\xi) - K_\partial(\phi))\sigma\left(\frac{\xi/\hat{s}_\phi - \chi_\mathrm{m}}{\delta_K}\right) + K_\partial(\phi)\,\mathrm{d}\phi. \tag{S4}$$

Using the fit parameters $\varsigma = 1.71$, $\omega = 3$, $\chi_\mathrm{m} = 0.38$, and $\delta_K = 0.096$ determined from the aggregated data in Figs. 4(a) and (b), the predicted hindrance functions obtained from Eq. (S4) via numerical integration are quite consistent with the original data for any parameter combinations, as shown in Fig. S4. Some deviation from the data is visible for $\lambda_\mathrm{D} = 5\,\text{nm}$, where a slightly slower decrease of v is observed compared to the prediction by Eq. (S4). The most likely reason for this is the attractive van der Waals force in the simulation that is not taken into account by the simple potential barrier model behind K_Φ.

S6 Next-neighbor distances for non-interacting particles

Let the probability of finding the next neighbor of a particle of radius R at center-to-center distance $c_{\mathrm{nn}} = s_{\mathrm{nn}} + 2R$ in a monodisperse suspension of concentration $n = \phi/V_{\mathrm{p}}$ be $\mathcal{P}(c_{\mathrm{nn}})\,\mathrm{d}c$. We can write this probability as a product of the probability P_1 that no other particle is within $c < c_{\mathrm{nn}}$ of the particle and the probability P_2 that there is a particle in the infinitesimal range $[c_{\mathrm{nn}}, c_{\mathrm{nn}} + \mathrm{d}c]$,

$$\mathcal{P}(c_{\mathrm{nn}})\,\mathrm{d}c = \underbrace{\Big(1 - \int_{2R}^{c_{\mathrm{nn}}} \mathcal{P}(c)\,\mathrm{d}c\Big)}_{P_1} \times \underbrace{4\pi n c_{\mathrm{nn}}^2\,\mathrm{d}c}_{P_2}. \tag{S5}$$

We let the integration in P_1 commence at $c = 2R$ because we can assume that $\mathcal{P}(c < 2R) = 0$ due to hard sphere repulsion. By canceling the remaining $\mathrm{d}c$ and deriving by c_{nn} on both sides we arrive at the differential equation

$$\frac{\partial \mathcal{P}(c_{\mathrm{nn}})}{\partial c_{\mathrm{nn}}} = \mathcal{P}(c_{\mathrm{nn}})\Big(\frac{2}{c_{\mathrm{nn}}} - 4\pi n c_{\mathrm{nn}}^2\Big). \tag{S6}$$

This differential equation is solved by

$$\mathcal{P}(c_{\mathrm{nn}}) = 4\pi n c_{\mathrm{nn}}^2 e^{-\frac{4}{3}\pi n (c_{\mathrm{nn}}^3 - 8R^3)}, \tag{S7}$$

which fulfills the normalization condition

$$\int_{2R}^{\infty} \mathcal{P}(c)\,\mathrm{d}c = 1. \tag{S8}$$

The average distance to the next neighbor $\langle \hat{s}_{\mathrm{nn}} \rangle = \langle c_{\mathrm{nn}} \rangle / R - 2$ and the standard deviation $\Delta \hat{s}_{\mathrm{nn}}$ can be computed from the first and second moments of $\mathcal{P}$ via numerical integration.